SiGeC/Si Electrooptic Modulators

Martin F. Schubert, *Student Member, IEEE*, and Farhan Rana, *Member, IEEE*

***Abstract*—The addition of carbon to silicon-germanium alloys provides the ability to lattice match thick layers with high germanium composition to silicon substrates. Thick strain-free silicon-germanium-carbon (SiGeC) layers on silicon allow the design of optical waveguides that have large optical mode overlap with the waveguide core. In addition, SiGeC/Si heterostructures enable strong confinement of large electron and hole concentrations. The combination of tightly confined carriers and photons can be used to realize high-performance broadband electrooptic modulators based on carrier density-induced refractive index changes. We show that modulators with lengths around 30 μm and turn-on times below 0.2 ns are possible with optimized designs.**

***Index Terms*—Device modeling, integrated optics, optical modulator, plasma dispersion effect, silicon optoelectronics.**

I. Introduction

THE ADVANTAGES of CMOS-compatible manufacturing and promise of integration with advanced electronics have made the silicon material system an attractive target for photonic system applications. Both all-silicon and silicon-germanium electrooptic modulators have been demonstrated [1]–[27]. These devices typically employ the plasma dispersion effect, in which injected carrier density induces change in the refractive index. Modulators based upon the plasma dispersion effect require a good overlap of the optical mode with the region where large carrier concentrations are injected.

In the all-silicon platform, it is difficult to build low-loss structures that tightly confine both the optical mode and injected carriers. Silicon p-i-n homojunction modulators—which constitute the bulk of all-silicon modulators—often require degenerate or nearly degenerate doping to enable high carrier concentrations in the intrinsic region. Keeping the optical mode away from such highly doped layers as well as metal contacts and etched surfaces requires careful design to keep modal loss small [1]. Additionally, the silicon-on-insulator (SOI) waveguide designs that are typically used suffer from poor thermal characteristics at high current levels as a result of the low-thermal conductivity oxide layer below the active region. As a result, maximum performance in all-silicon modulators has been achieved with microcavity resonator designs [1]–[6]. Resonator-based modulators require much lower currents for operation and generate less heat as a result. However, microcavity resonator modulators inherently suffer from narrow optical bandwidth. Broadband SOI modulators are typically limited in speed or have long device lengths [7]–[18].

Although SiGe/Si heterostructures have the potential to meet the challenges mentioned above, the large lattice mismatch between germanium and silicon results in very small values for the critical thickness of epitaxial layers. Consequently, the results for SiGe modulators that have been reported in the literature suffer from small optical confinement factors, long device lengths, and small RC limited bandwidths [19]–[26].

In this paper, we show that silicon-germanium-carbon (SiGeC) alloy heterostructures can be used to design optical waveguides that can confine both the injected carriers and the optical mode to the waveguide core, thereby offering opportunities for realizing high-performance compact broadband electrooptic phase/intensity modulators on silicon. SiGeC alloys have been around for more than 10 years and have been used to make various electronic devices such as heterojunction bipolar transistors and thermoelectric coolers [27], [28]. The optical properties of these alloys have been extensively studied [29]–[31], and the authors are aware of at least one published result that demonstrated optical waveguiding in these alloys [32]. SiGeC/Si heterostructures have also been used in waveguide photodetectors [33]–[35]. In this paper, we examine SiGeC as the active region material in p-i-n heterostructure electrooptic modulators.

This paper is organized as follows. Section II describes the model for SiGeC optical properties including refractive index and interband absorption. Section III discusses optimization of the waveguide design. Section IV treats modulator high speed switching performance and device length. Section V gives concluding remarks.

II. Material Properties

A. Critical Thickness

Achieving high-performance SiGeC electrooptic modulators relies upon the ability to grow thick high-quality epitaxial layers. Pseudomorphic, dislocation-free layers can generally be grown up to the critical thickness h_c. Different models for h_c exist, but a conservative estimate is obtained by the Matthews–Blakeslee formula for capped layers [36]

$$h_c = \frac{b}{4\pi f}\left[\frac{1-\nu}{1+\nu}\frac{\cos^2\theta}{\cos\lambda}\right]\ln\left(\frac{h_c}{b}\right) \tag{1}$$

where b is the Burger's vector modulus, λ is the angle of the Burger's vector, ν is Poisson's ratio, θ is the dislocation angle, and f is the substrate-alloy misfit parameter. Fig. 1 plots the

Manuscript received July 25, 2006; revised November 2, 2006. This work was supported by the National Science Foundation and the Lawrence Semiconductor Research Laboratory, Inc.

M. F. Schubert is with the Electrical, Computer, and Systems Engineering Department, Rensselaer Polytechnic Institute, Troy, NY 12180 USA (e-mail: mfs24@cornell.edu; schubm@rpi.edu).

F. Rana is with the Department of Electrical and Computer Engineering, Cornell University, Ithaca, NY 14853 USA (e-mail: fr37@cornell.edu).

Color versions of one or more of the figures in this paper are available online at http://ieeexplore.ieee.org.

Digital Object Identifier 10.1109/JLT.2006.890432

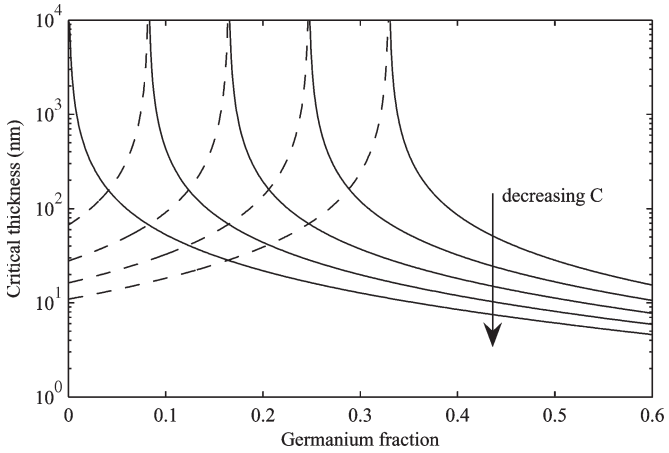

Fig. 1. Critical thickness of $Si_{1-x-y}Ge_xC_y$ as a function of germanium content for carbon fractions of 0.04, 0.03, 0.02, 0.01, and 0. Solid curves are for alloys that are compressively strained, whereas dashed lines are for tensile strain.

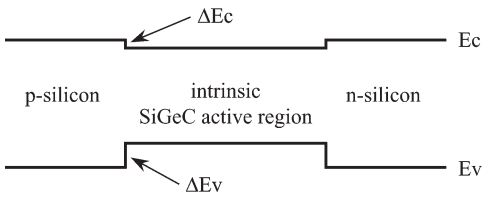

Fig. 2. Band diagram for a typical SiGeC p-i-n heterostructure.

Matthews–Blakeslee critical thickness of SiGeC as a function of the germanium and carbon fractions. A Ge:C ratio of 8.5 : 1 results in a layer lattice matched to silicon. The experimentally observed thicknesses of defect-free SiGeC layers have been found to follow the Matthews–Blakeslee formula for carbon fractions less than 0.04 and for Ge:C ratios higher than 8.5 : 1 [37]. Outside these limits SiGeC epitaxial layers tend to develop defects and may even become amorphous [37]. SiGeC layers with carbon fractions between 0.02 and 0.03 have been grown to thicknesses greater than 0.5 μm with good crystal quality [32]. As we will show later, the optimal thickness for SiGeC layers tends to be between 0.2 and 0.3 μm, which is well within the limits of current techniques to grow SiGeC epitaxial layers.

B. Band Offsets and Carrier Confinement

The conduction and valence band profile of the proposed Si-SiGeC-Si electrooptic modulator waveguide is shown in Fig. 2. The conduction band offset between Si and $Si_{1-x-y}Ge_xC_y$ for small carbon fractions is given approximately by the relation [38]

$$\Delta E_{\rm C} = -0.09x - 0.5y \tag{2}$$

and the heavy hole valence band offset is given as [38]

$$\Delta E_V = 0.82x - 2.6y. \tag{3}$$

Note that the addition of carbon helps to increase the conduction band offset between Si and SiGeC compared to that between Si and SiGe. As we will show later, optimal modulator designs typically include germanium and carbon fractions greater than 0.25 and 0.03, respectively. For such a design the conduction band offset is close to 40 meV, and the valence band offset is close to 130 meV. Such large band offset values are adequate to confine the injected electrons and holes in the waveguide active region. We discuss charge confinement in more detail in Section IV.

C. Refractive Index

The authors are not aware of any systematic experimental measurements of the refractive index of SiGeC alloys. The refractive index model—used previously in [32]—depends only on the bandgap of the alloy and the indexes of bulk silicon and germanium. In this paper, the refractive index of a SiGeC layer is assumed to be identical to that of a SiGe layer with the same bandgap. The refractive index of SiGe is given by a linear model used in [39]. Using (2) and (3) with the linear index model for SiGe yields

$$n_{Si_{1-x-y}Ge_xC_y} = n_{\rm Si} + (n_{\rm Ge} - n_{\rm Si})\left(x - \frac{2.1}{0.9}y\right). \tag{4}$$

Dependence of the refractive index and free carrier absorption on the presence of free electrons and holes is assumed to be identical to that in silicon as given in [40]. At 1550 nm, the change in the refractive index and absorption is given by

$$\Delta n = -1.7 \times 10^{-22}(N_{\rm e})^{1.04} - 3.9 \times 10^{-18}(N_{\rm h})^{0.818} \tag{5}$$

$$\Delta\alpha = 2.0 \times 10^{-21}(N_{\rm e})^{1.20} + 3.5 \times 10^{-20}(N_{\rm h})^{1.12} \tag{6}$$

where $\Delta\alpha$ is in units of cm^{-1}. $N_{\rm e}$ and $N_{\rm h}$ are the electron and hole concentrations in units of cm^{-3}. At 1300 nm Δn and $\Delta\alpha$ are given by

$$\Delta n = -7.9 \times 10^{-23}(N_{\rm e})^{1.05} - 4.8 \times 10^{-18}(N_{\rm h})^{0.805} \tag{7}$$

$$\Delta\alpha = 1.1 \times 10^{-20}(N_{\rm e})^{1.15} + 3.8 \times 10^{-20}(N_{\rm h})^{1.11}. \tag{8}$$

D. Material Interband Absorption

High germanium content in core layer can lead to large material absorption at near-IR wavelengths. In this paper, material absorption is calculated using a model for phonon-assisted indirect optical transitions similar to one used previously for SiGe [39], [41]. The absorption coefficient is given by

$$\alpha = 0 \quad \hbar\omega \le E_g - k\theta \tag{9a}$$

$$= A_{\rm a}\frac{[\hbar\omega - E_g + k\theta]^2}{\exp(\theta/T) - 1} \quad E_g - k\theta < \hbar\omega < E_g + k\theta \tag{9b}$$

$$= A_{\rm a}\frac{[\hbar\omega - E_g + k\theta]^2}{\exp(\theta/T) - 1} + A_{\rm e}\frac{[\hbar\omega - E_g - k\theta]^2}{1 - \exp(-\theta/T)} \quad \hbar\omega \ge E_g + k\theta. \tag{9c}$$

Here, E_g is the indirect bandgap, T is the temperature, and θ is the phonon equivalent temperature. $A_{\rm a}$ and $A_{\rm e}$ are proportionality factors for the processes of phonon absorption and phonon emission, respectively. The parameters θ, $A_{\rm a}$, and $A_{\rm e}$ are extracted from experimental absorption results for SiGe alloys [41]. The effect of carbon and strain is neglected with the

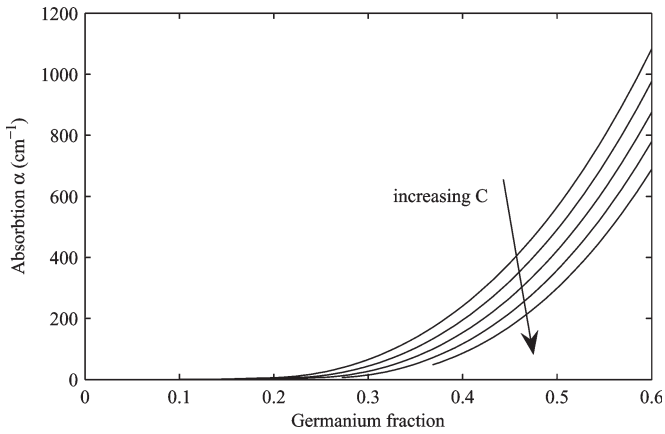

Fig. 3. Optical absorption coefficient of $Si_{1-x-y}Ge_xC_y$ at 1300 nm as a function of germanium content for carbon fractions of 0, 0.01, 0.02, 0.03, and 0.04.

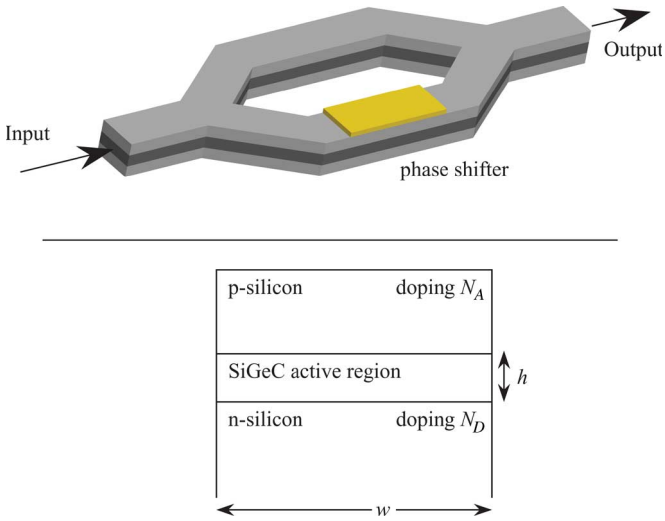

Fig. 4. (Above) Schematic cross-sectional view of the p-i-n diode Mach–Zehnder electrooptic modulator. (Below) Cross-sectional view of the p-i-n diode Mach–Zehnder electrooptic modulator. The intrinsic active region has height h and width w; only the vertical direction is considered in simulations.

exception of the modification to the bandgap. Fig. 3 plots the modeled absorption coefficient as a function of composition.

III. Modulator Active Region Design

A. SiGeC Modulator Design Considerations

We consider Mach–Zehnder broadband electrooptic modulators operating at 1550 and 1300 nm. In this paper, simulations are 1-D and directly treat only the vertical direction of the p-i-n heterostructure modulator; results are extended to 2-D by assuming a device width. The basic device design is shown in Fig. 4. The Mach–Zehnder interferometer design converts phase modulation in one arm of the interferometer to amplitude/intensity modulation at the output. To achieve good modulation depth a phase shift close to π is needed in one arm of the interferometer with respect to the other arm. Operation of the modulator is based on carrier density-induced refractive index change (plasma dispersion effect) in semiconductors [40]. The waveguide geometry consists of a core SiGeC intrinsic layer

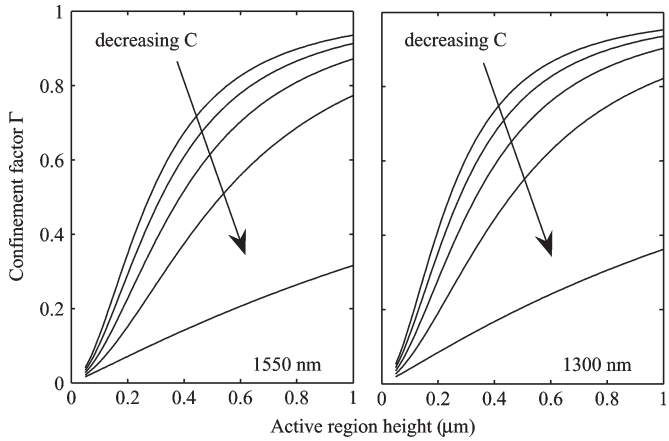

Fig. 5. Active region confinement factor Γ at (left) 1550 nm and (right) 1300 nm with carbon composition of 0.04, 0.03, 0.02, 0.01, and 0.

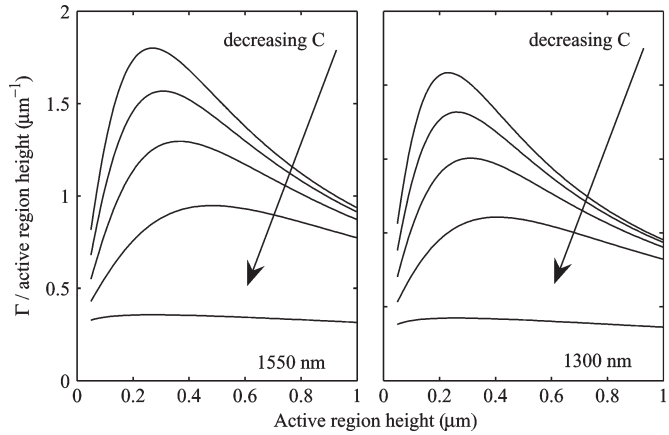

Fig. 6. Figure-of-merit Γ/h for the modulator at (left) 1550 nm and (right) 1300 nm with carbon composition y of 0.04, 0.03, 0.02, 0.01, and 0.

that is sandwiched between n- and p-doped Si cladding layers. The core layer helps to confine both the injected carriers as well as the optical mode. Modulator performance is characterized by the modulator length and the switching current needed to achieve a π phase shift. Minimizing current is critical because large switching currents cause heating which changes the refractive index in silicon by as much as $+2 \cdot 10^{-4}$ per degree and counteracts the carrier-induced refractive change [42]. Minimizing device length is important in order to avoid modulation bandwidth reduction due to RC effects.

The total phase shift accumulated during propagation through one arm of the modulator is given by

$$\Delta\phi = \frac{2\pi}{\lambda}\Gamma\Delta n_{\text{act}}L \tag{10}$$

where Γ is the optical confinement factor for the waveguide core, L is the length, λ is the wavelength, and Δn_{act} is the change in refractive index of the active region due to carrier injection. The device switch-on dynamics are determined by carrier injection and subsequent carrier diffusion in the core layer under an applied forward bias. The switch-off dynamics are governed by carrier sweep out in an electric field under an applied reverse bias. With equal injection of electrons and holes and carrier recombination and leakage out of the active

TABLE I
PARAMETERS FOR OPTIMIZED SiGeC MODULATOR DESIGNS AT 1550 AND 1300 nm

λ (nm)	% carbon	% germanium	core height (μm)	Γ	Γ/h (μm^{-1})
1550	0.0	2.51	0.28	0.10	0.36
1550	1.0	9.84	0.48	0.45	0.95
1550	2.0	18.5	0.37	0.48	1.30
1550	3.0	27.1	0.31	0.49	1.57
1550	4.0	35.6	0.27	0.49	1.80
1300	0.0	2.68	0.26	0.11	0.42
1300	1.0	10.1	0.41	0.45	1.11
1300	2.0	18.8	0.31	0.47	1.51
1300	3.0	27.5	0.26	0.47	1.82
1300	4.0	36.0	0.23	0.48	2.08

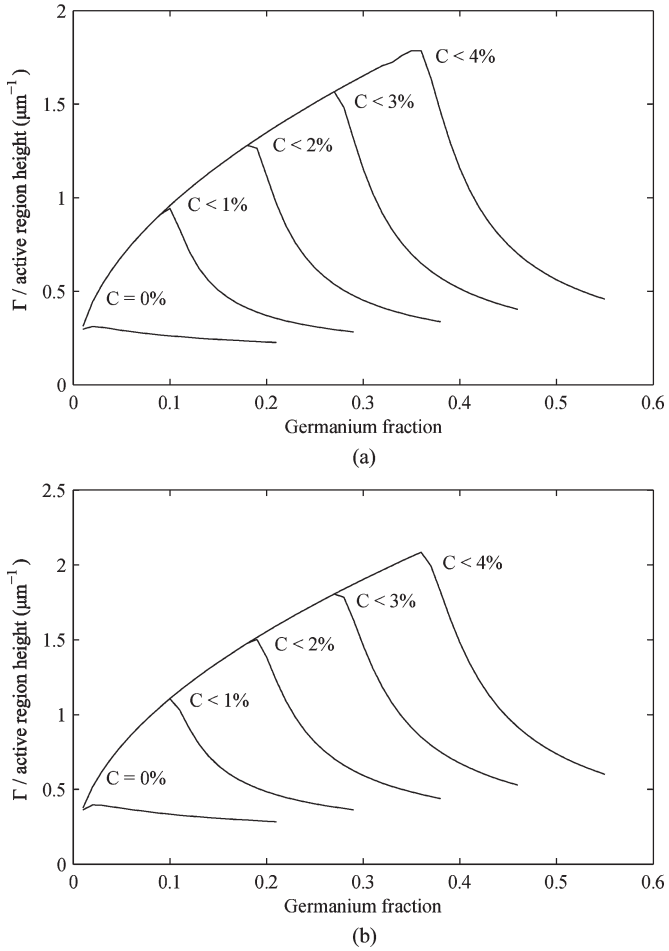

Fig. 7. Γ/h at (a) 1550 nm and (b) 1300 nm as a function of the active region composition.

region neglected, an injected current level I will result in carrier concentrations $N_{\rm e}$ and $N_{\rm h}$ given approximately by

$$N_{\rm h} = N_{\rm e} = \frac{1}{q}\frac{I}{hwL}t. \tag{11}$$

Here, h and w are the active region height and width, and t is current injection time. From (5) and (7), the change in index is nearly linearly related to the carrier concentration. Assuming charge neutrality ($N_{\rm h} = N_{\rm e} = N$), $\Delta n_{\rm act}$ can be written as

$$\Delta n_{\rm act} \approx -fN \tag{12}$$

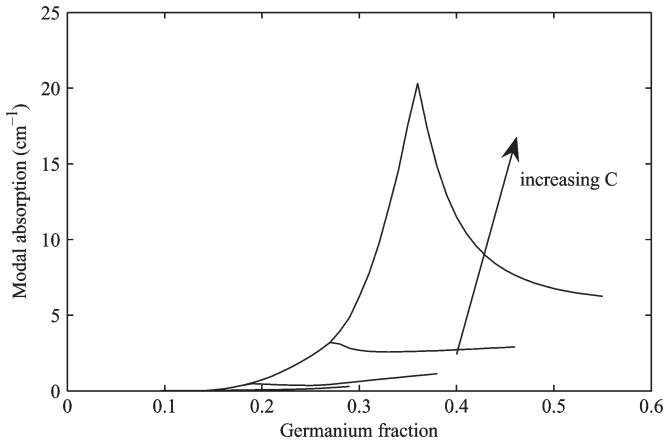

Fig. 8. Modal absorption for modulators at 1300 nm as a function of composition.

where f has a value of 2.96×10^{-21} cm^3 and 2.11×10^{-21} cm^3 for $N = 10^{18}$ cm^{-3} at 1550 and 1300 nm, respectively. Together with (10)–(12) yields

$$\Delta\phi \approx \frac{2\pi}{\lambda}\frac{\Gamma}{hw}\frac{1}{q}fIt. \tag{13}$$

Equation (13) shows that for a given current level, the turn-on time is minimized by maximizing Γ/hw. Similarly, for a desired switching time, the current is reduced by increasing Γ/hw.

B. Optimized Modulator Active Region Designs

Fig. 5 shows the optical confinement factor calculated using a 1-D mode solver at 1550 and 1300 nm for the SiGeC waveguide core layer achievable for different carbon fractions as a function of the core layer height. For each carbon fraction and a core layer thickness value, the maximum germanium fraction allowed by critical thickness limitations is chosen. The range of compositions achievable by current growth techniques is not exceeded. Fig. 5 shows that the addition of carbon allows for confinement factor values that are much larger than what is achievable in pure SiGe designs.

As mentioned earlier, Γ/hw rather than Γ is the superior figure of merit for the electrooptic modulator. For the waveguide active region, we assume a width of 0.5 μm to achieve close to unity mode confinement in the horizontal direction. Fig. 6 plots

the dependence of Γ/h on the thickness of the core region for the same modulators considered in Fig. 5. As the core region height increases from small values, the confinement factor Γ increases rapidly, and so does the value of the ratio Γ/h. As the thickness of the core region increases further, the confinement factor increases more slowly, and beyond a certain thickness, the value of the ratio Γ/h decreases as the core layer thickness increases. The maximum value of the ratio Γ/h for different carbon fractions is seen to occur for values of the core layer thickness between 0.2 and 0.3 μm for carbon fractions of 0.02 to 0.04. The maximum value of the ratio Γ/h increases with the carbon fraction of the core layer because a larger carbon fraction allows higher germanium content, a higher core layer index, and therefore tighter optical mode confinement for a given thickness. Table I shows the parameters of the optimized modulators. Compared to modulators with SiGe core layers, SiGeC designs enable values of Γ/h that are larger by factor of as much as 5.

The effect of composition on the Γ/h parameter is more explicitly shown in Fig. 7, which plots Γ/h as a function of germanium composition for several values of carbon composition at 1550 and 1300 nm. For each germanium and carbon fraction, the core region thickness value is chosen such that the ratio Γ/h is maximized, and the limitations imposed by the critical thickness values are not exceeded. Fig. 7 shows that for high germanium compositions, small values of the critical thickness reduce the value of the ratio Γ/h. It would be desirable to raise the carbon content beyond 4%, which would allow higher germanium content and increase the value of Γ/h even further.

Material interband absorption also forms a barrier to achieving maximum performance. At 1550-nm, interband absorption plays an insignificant role since the photon energy is below the bandgap of the core layer. However, as shown earlier, germanium fractions larger than 0.3 can result in significant optical absorption at 1300 nm. Fig. 8 plots the net modal loss for the modulator waveguide at 1300 nm as a function of the germanium composition of the core layer for several values of the carbon composition. When the carbon fraction is above 0.03 and the germanium fraction is greater than 0.3, modal absorption can become significant and approaches values as high as 20 cm^{-1}. As a result, compositions which achieve the maximum Γ/h may be undesirable due to high insertion losses.

IV. Modulator High-Speed Performance

A. Current Injection and Charge Confinement

In a basic model for the electrical device characteristics, the carrier concentration in the modulator active region with an applied current I is given by

$$\frac{\partial N}{\partial t} = \frac{I}{qV} - \frac{N}{\tau_{\mathrm{SRH}}} - R_{\mathrm{Auger}}(N) - \frac{N}{\tau_{\mathrm{leak}}(N)} \tag{14}$$

where V is the total core region volume, τ_{SRH} is the Schockley–Reed–Hall carrier recombination lifetime, $R_{\mathrm{Auger}}(N)$ is the Auger recombination rate, and $\tau_{\mathrm{leak}}(N)$ is the carrier density dependent time constant associated with current leakage out of the active region due to thermionic emission. Leakage current is dominated by the electron thermionic emission current since the conduction band offsets between SiGeC and Si are much smaller than the valence band offsets. The Auger recombination rate was modeled using an expression given in [43].

Simulations to model current injection and carrier leakage were performed using the package SimWindows [44], which solves carrier transport equations self-consistently for semiconductor heterostructures in one dimension. Material parameters for SiGeC are somewhat unknown, but a good estimate is given by the parameters of bulk SiGe with the same germanium composition. The material properties used in simulations are shown in Table II. Because the high index waveguide core generally keeps the optical mode away from etched surfaces and metal contacts, the recombination lifetime was assumed to be 20 ns. An example of simulation results is shown in Figs. 9 and 10. Fig. 9 shows the band diagram of the 1550-nm optimized modulator with a carbon composition of 0.03. The applied voltage is 0.80 V in forward bias, which results in a steady-state carrier concentration in the active region of $N = N_{\mathrm{e}} = N_{\mathrm{h}} = 1.27 \times 10^{18}$. Fig. 10 plots the electron and hole current density as a function of position in the device. The minority carrier currents on either side of the junction constitute the leakage current. The tight confinement of carriers by the SiGeC/Si heterostructure is shown by the large amount of recombination that takes place in the modulator active region. Only a small fraction of the injected carriers leak out of the core region.

To find the values of τ_{leak} we considered SiGeC p-i-n heterojunctions with an applied voltage. For value of the applied voltage the minority carrier current density on each side of the p-i-n junction and the carrier concentration N in the active region are obtained. The total minority carrier current density is a good estimate of the current which leaks out of the active region J_{leak}. The electron and hole density leaving the active region are each given by J_{leak}/qh, which must be equal to the leakage term in (14). This yields

$$\tau_{\mathrm{leak}}(N) = \frac{qhN}{J_{\mathrm{leak}}}. \tag{15}$$

The carbon and germanium fractions of the core layer, as well as the doping in the claddings on the n- and p-sides of the device, can play a significant role in determining the leakage lifetime. Fig. 11 plots τ_{leak} at a carrier density of $N = 1 \times 10^{18}$ cm^{-3} for various doping levels in the n-cladding with varying carbon fractions in the waveguide core. The active region compositions and sizes are the optimized values shown in Table I. The acceptor doping level in the p-cladding is twice the doping level in the n-cladding to minimize electron leakage current. Increasing the carbon content (and, therefore, the germanium content) increases carrier confinement and significantly increases the carrier leakage time constant. Increasing the doping level in the cladding also substantially decreases carrier leakage. However, the decrease in leakage must be balanced against the increased free carrier absorption that arises from higher doping levels in the cladding. When the donor

TABLE II
MATERIAL PARAMETERS USED FOR THE SIMULATION OF SiGeC. FOR GERMANIUM FRACTIONS LARGER THAN 0.3, MOBILITIES OF 102 AND 191 $cm^2/V \cdot s$ WERE USED FOR THE ELECTRONS AND HOLES. THE CHOICE OF ELECTRON AND HOLE SCHOCKLEY–READ–HALL LIFETIMES RESULTS FROM THE VALUE OF τ_{SRH}

Parameter	Si	$Si_{1-x-y}Ge_xC_y$	Units	Ref.
Bandgap	1.12	1.12 – 0.90x + 2.1y	eV	38
Electron Affinity	4.05	4.05 + 0.09x + 0.5y	eV	38
Dielectric constant	11.7	11.7 + 4.5x		45
Electron mobility	1396	1396 – 4315x*	cm^2/Vs	45
Electron conductivity effective mass	0.26	0.26	m_0	46
Electron density of states effective mass	1.08	1.08	m_0	46
Electron Shockley-Reed-Hall lifetime	10	10	ns	
Hole mobility	450	450 – 865x*	cm^2/Vs	45
Hole conductivity effective mass	0.386	0.386 – 0.176x	m_0	47
Hole density of states effective mass	0.81	0.81 – 0.52x	m_0	47
Hole Shockley-Reed-Hall lifetime	10	10	ns	

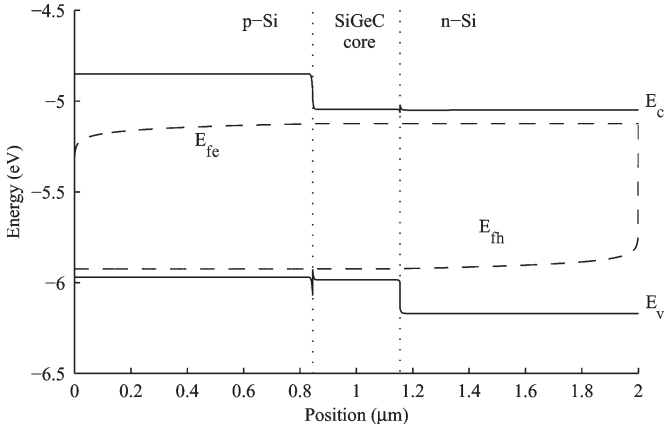

Fig. 9. Bands as a function of position for the 1550-nm optimized modulator with carbon content of 0.03 and a 0.80-V forward bias applied.

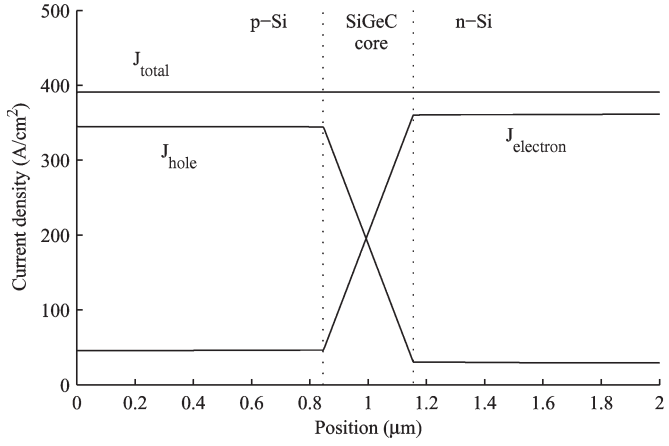

Fig. 10. Electron and hole current density as well as total current density as a function of position for the 1550-nm optimized modulator with 0.03 carbon and a 0.80-V forward bias.

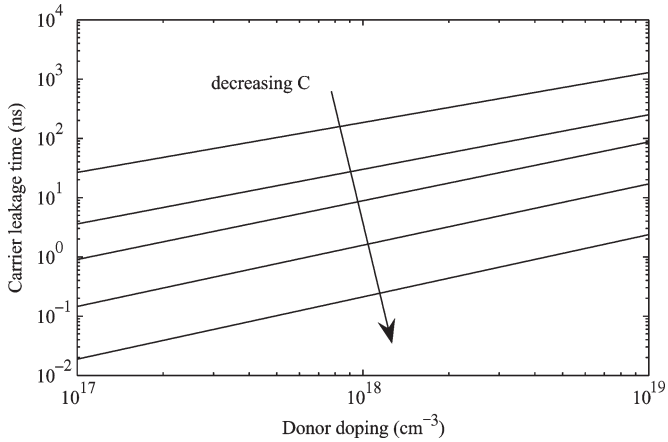

Fig. 11. Carrier leakage lifetime at a carrier concentration $N = 1 \times 10^{18}$ cm^{-3} for the 1550-nm optimized modulators with various carbon contents as a function of the donor doping N_d. Acceptor doping N_a is held at twice N_d.

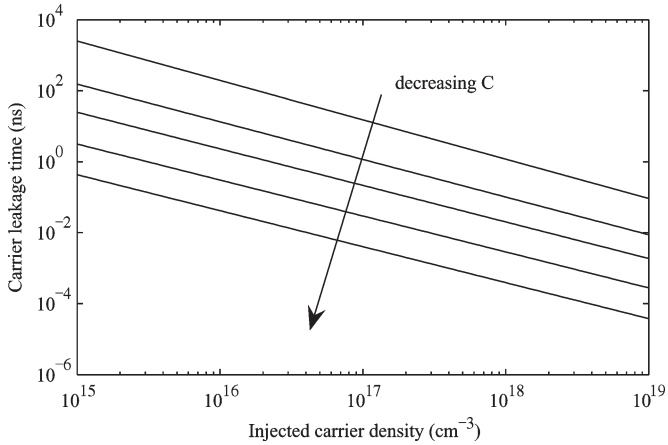

Fig. 12. Carrier leakage lifetime as a function of carrier concentration for 1550-nm optimized modulators with carbon contents of 0.04, 0.03, 0.02, 0.01, and 0. $N_d = 1.5 \times 10^{18}$; $N_a = 3.0 \times 10^{18}$.

doping is kept below 1.5×10^{18} cm^{-3}, the insertion loss in a 500-μm modulator is kept below 1 dB. Fig. 12 shows the carrier leakage time constant as a function of the carrier concentration in the core layer for the 1550-nm optimized designs. Doping levels of 1.5×10^{18} and 3.0×10^{18} cm^{-3} were chosen for the n- and p-sides of the device.

B. Switching Speed and Modulator Length

Equation (14) is adequate to describe the time dependence of the carrier injection process in the core region since carrier transport affects, such as diffusion of the injected carriers to

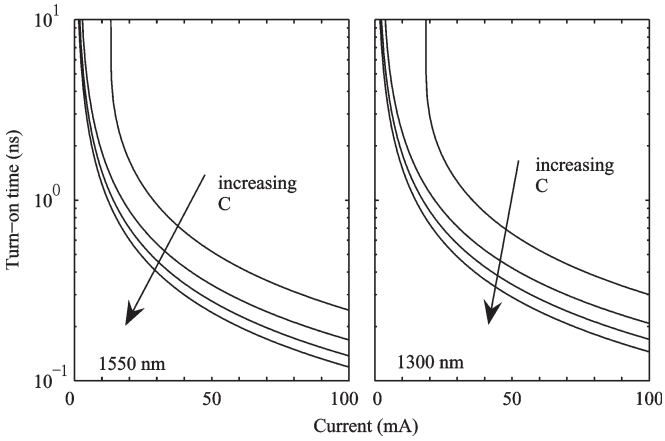

Fig. 13. Turn-on time of 500-μm modulators at (left) 1550 nm and (right) 1300 nm with carbon fractions of 0.01, 0.02, 0.03, and 0.04. The device width is 0.5 μm.

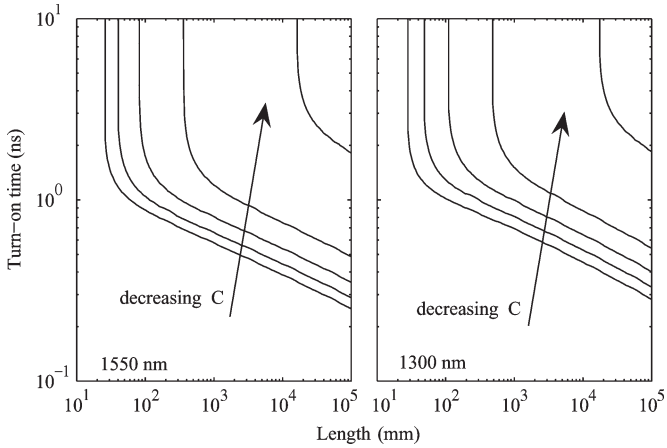

Fig. 14. Turn-on time of optimized modulators for a 20-mA current at (left) 1550 nm and (right) 1300 nm as a function of the modulator length with carbon fractions of 0.04, 0.03, 0.02, 0.01, and 0.

fill the core region, happen on much shorter time scales. For example, the hole diffusion process is expected to take time on the order of $h^2/2D_{\rm h}$ to fill the core region of thickness h. Here, $D_{\rm h}$ is the hole diffusivity. Using a typical value of 10 cm^2/s for the hole diffusivity in SiGe [29], the time taken by holes to diffuse across a 0.2-μm-thick region is found to be less than 20 ps. Therefore, the turn-on time for the modulator is found by simply solving (14) for the time at which the injected carrier density and resultant index change are large enough to achieve a π phase shift for a given device length. Fig. 13 plots the turn-on time of the optimized modulators from Table I with 500-μm length at 1550 and 1300 nm as a function of the current injection level. This turn-on time is expected to be the limiting component determining the switching speed of SiGeC modulators. Turn-off time is the time needed to remove the carriers from the active region, which is accomplished by reverse biasing the device and can be fast [1]. Simulated carrier sweep-out times in [1] are less than 0.2 ns for an SOI modulator with a 0.5-μm-wide junction. Unlike the modulators in [1], the SiGeC devices considered here have core region widths that are typically less than 0.3 μm for modulators with carbon content greater than 0.02. The device geometry also helps to generate strong well-confined electric fields in the core layer under a reverse bias compared to SOI geometries [1]. These two factors are expected to decrease the turn-off time of SiGeC modulators compared to SOI designs. As a result, we expect that the bandwidth of the device will not be limited by the switch-off time.

Achieving a π phase shift in shorter device lengths requires a larger refractive index change in the active region, which is accomplished by increasing the injected carrier concentration. However, as the refractive index is reduced further by injecting more carriers, the optical mode confinement factor decreases, which necessitates an even-larger refractive index change. In addition, as the carrier concentration rises, the Auger rate and carrier leakage from the active region also increase. As a result, the current required to achieve the desired carrier concentration can be large for short device lengths. Fig. 14 plots the switching time for modulators with a 20-mA total injected current as a function of the modulator length for the optimized modulators from Table I. Fig. 14 shows that for carbon fractions larger than 0.02, sub-100-μm modulator device lengths are possible with switching times around 1 ns. For larger carbon fractions, lengths approaching 20 μm are achievable. The small device lengths are achieved as a result of both the optical mode confinement and the charge confinement provided by the SiGeC/Si heterostructures. The minimum length for designs with carbon fractions below 0.02 is determined by leakage current. For devices with carbon concentrations of 0.02 and above, the leakage current is much smaller, and the length is instead limited by the strong increase in Auger recombination at high carrier concentrations as well as the reduction in optical mode confinement factor.

In practice, the smallest achievable device size is expected to be determined by thermal effects. The calculations for turn-on times in Fig. 14 do not consider device heating from current injection. Device heating would result from carrier recombination and from I^2R losses at the ohmic contacts. Ohmic contact resistance becomes larger as the device length decreases. For small device lengths, large current densities and contact resistances are expected to cause significant heating, which will ultimately place a limit on the modulator length. Three-dimensional device simulations that take into account heat generation and diffusion are required to study thermal effects in short devices and are left for later work. However, because of the absence of a high thermal impedance oxide layer that is present in SOI devices [1], heat dissipation is expected to be less of a problem in SiGeC modulators.

V. Conclusion

We have proposed and analyzed optically broadband electrooptic modulators based upon the SiGeC/Si material system. SiGeC can be lattice-matched to silicon, which allows for thick layers with large germanium content that can be used to achieve high optical mode confinement in optical waveguides. Additionally, the band offset between Si and SiGeC strongly confine carriers to the waveguide core, which results in strong

overlap between large injected carrier concentrations and the optical mode. We show that SiGeC/Si modulators with lengths around 30 μm and turn-on times approaching 0.2 ns are possible with optimized designs.

REFERENCES

[1] C. A. Barrios, V. R. Almeida, R. Panepucci, and M. Lipson, "Electro-optic modulation of silicon-on-insulator submicrometer-size waveguide devices," *J. Lightw. Technol.*, vol. 21, no. 10, p. 2332, Oct. 2003.

[2] X. Xiao, J. C. Sturm, K. K. Goel, and P. V. Schwartz, "Fabry–Pérot optical intensity modulator at 1.3 μm in silicon," *IEEE Photon. Technol. Lett.*, vol. 3, no. 3, p. 230, Mar. 1991.

[3] M. Y. Liu and S. Chou, "High-modulation-depth and short-cavity-length silicon Fabry–Pérot modulator with two grating Bragg reflectors," *Appl. Phys. Lett.*, vol. 68, no. 2, pp. 170–172, Jan. 1995.

[4] A. Cutolo, M. Iodice, A. Irace, P. Spirito, and L. Zeni, "An electrically controlled Bragg reflector integrated in a rib silicon on insulator waveguide," *Appl. Phys. Lett.*, vol. 71, no. 2, pp. 199–201, Jul. 1997.

[5] C. A. Barrios, V. R. Almeida, and M. Lipson, "Low-power-consumption short-length and high-modulation-depth silicon electrooptic modulator," *J. Lightw. Technol.*, vol. 21, no. 4, pp. 1089–1098, Apr. 2003.

[6] G. Coppola, A. Irace, M. Iodice, and A. Cutolo, "Simulation and analysis of a high-efficiency silicon optoelectronic modulator based on a Bragg mirror," *Opt. Eng.*, vol. 40, no. 6, pp. 1076–1081, Jun. 2001.

[7] J. P. Lorenzo and R. A. Soref, "1.3 μm electro-optic silicon switch," *Appl. Phys. Lett.*, vol. 51, no. 1, pp. 6–8, Jul. 1987.

[8] B. R. Hemenway, O. Solgaard, and D. M. Bloom, "All-silicon integrated optical modulator for 1.3 μm fiber-optic interconnects," *Appl. Phys. Lett.*, vol. 55, no. 4, pp. 349–350, Jul. 1989.

[9] G. V. Treyz, P. G. May, and J.-M. Halbout, "Silicon optical modulators at 1.3 μm based on free-carrier absorption," *IEEE Electron Device Lett.*, vol. 12, no. 6, pp. 276–278, Jun. 1991.

[10] ——, "Silicon Mach–Zehnder waveguide interferometers based on the plasma dispersion effect," *Appl. Phys. Lett.*, vol. 59, no. 7, p. 771, 1991.

[11] Y. L. Liu, E. K. Liu, S. L. Zhang, G. Z. Li, and J. S. Luo, "Silicon 1×2 digital optical switch using plasma dispersion," *Electron. Lett.*, vol. 30, no. 2, pp. 130–131, Jan. 1994.

[12] Y. L. Liu, E. Liu, G. Li, S. Zhang, J. Luo, F. Zhou, M. Cheng, B. Li, and H. Ge, "Novel silicon waveguide switch based on total internal reflection," *Appl. Phys. Lett.*, vol. 64, no. 16, pp. 2079–2080, 1994.

[13] C. Z. Zhao, G. Z. Li, E. K. Liu, Y. Gao, and X. D. Liu, "Silicon on insulator Mach–Zehnder waveguide interferometers operating at 1.3 μm," *Appl. Phys. Lett.*, vol. 67, no. 17, pp. 2448–2449, Oct. 1995.

[14] C. Z. Zhao, E. K. Liu, G. Z. Li, Y. Gao, and C. S. Guo, "Zero-gap directional coupler switch integrated into a silicon-on-insulator for 1.3-μm operation," *Opt. Lett.*, vol. 21, no. 20, p. 1664, Oct. 1996.

[15] A. Cutolo, M. Iodice, P. Spirito, and L. Zeni, "Silicon electro-optic modulator based on a three terminal device integrated in a low-loss single-mode SOI waveguide," *J. Lightw. Technol.*, vol. 15, no. 3, pp. 505–518, Mar. 1997.

[16] C. Z. Zhao, A. H. Chen, E. K. Liu, and G. Z. Li, "Silicon-on-insulator asymmetric optical switch based on total internal reflection," *IEEE Photon. Technol. Lett.*, vol. 9, no. 8, pp. 1113–1115, Aug. 1997.

[17] A. Liu, R. Jones, L. Liao, D. Samara-Rubio, D. Rubin, O. Cohen, R. Nicolaescu, and M. Paniccia, "A high-speed silicon optical modulator based on a metal–oxide–semiconductor capacitor," *Nature*, vol. 427, no. 6975, pp. 615–618, Feb. 2004.

[18] V. R. Almeida, Q. Xu, and M. Lipson, "Ultrafast integrated semiconductor optical modulator based on the plasma-dispersion effect," *Opt. Lett.*, vol. 30, no. 18, pp. 2403–2405, 2005.

[19] O. Qasaimeh, J. Singh, and P. Bhattacharya, "Electroabsorption and electrooptic effect in SiGe-Si quantum wells: Realization of low-voltage optical modulators," *IEEE J. Quantum Electron.*, vol. 33, no. 9, pp. 1532–1536, Sep. 1997.

[20] O. Qasaimeh, P. Bhattacharya, and E. T. Croke, "SiGe-Si quantum-well electroabsorption modulators," *IEEE Photon. Technol. Lett.*, vol. 10, no. 6, pp. 807–809, Jun. 1998.

[21] B. Li, G. Li, E. Liu, Z. Jiang, J. Qin, and X. Wang, "Monolithic integration of a SiGe/Si modulator and multiple quantum well photodetector for 1.55 μm operation," *Appl. Phys. Lett.*, vol. 73, no. 24, pp. 3504–3505, Dec. 1998.

[22] A. Vonsovici and L. Vescan, "Modulation doped SiGe-Si MQW for low-voltage high-speed modulators at 1.3 μm," *IEEE J. Sel. Top. Quantum Electron.*, vol. 4, no. 6, pp. 1011–1019, Nov./Dec. 1998.

[23] B. Li, G. Li, E. Liu, Z. Jiang, C. Pei, and X. Wang, "1.55 μm reflection-type optical waveguide switch based on SiGe/Si plasma dispersion effect," *Appl. Phys. Lett.*, vol. 75, no. 1, p. 1, Jul. 1999.

[24] B. Li, Z. Jiang, X. Zhang, X. Wang, J. Wan, G. Li, and E. Liu, "SiGe/Si Mach–Zehnder interferometer modulator based on the plasma dispersion effect," *Appl. Phys. Lett.*, vol. 74, no. 15, pp. 2108–2109, Apr. 1999.

[25] D. Marris, A. Cordat, D. Pascal, A. Koster, E. Cassan, L. Vivien, and S. Laval, "Design of a SiGe-Si quantum-well optical modulator," *IEEE J. Quantum Electron.*, vol. 9, no. 3, pp. 747–754, May/Jun. 2003.

[26] D. Marries, E. Cassan, L. Vivien, D. Pascal, A. Koster, and S. Laval, "Design of a modulation-doped SiGe/Si optical modulator integrated in a submicrometer silicon-on-insulator waveguide," *Opt. Eng.*, vol. 4, no. 8, pp. 084 001–084 002, Aug. 2005.

[27] S. C. Jain and M. Willander, *Silicon-Germanium Strained Layers and Heterostructures*. New York: Academic, 2003.

[28] X. Fan, G. Zeng, C. LaBounty, and J. E. Bowers, "SiGeC/Si superlattice microcoolers," *Appl. Phys. Lett.*, vol. 78, no. 11, pp. 1580–1582, Mar. 2001.

[29] S. Zollner, "Optical properties and band structure of unstrained and strained $Si_{1-x}Ge_x$ and $Si_{1-x-y}Ge_xC_y$ alloys," in *Silicon-Germanium-Carbon Alloys*, S. T. Pantellides and S. Zollner, Eds. New York: Taylor and Francis, 2002.

[30] R. A. Soref, "Silicon based group IV heterostructures for optoelectronic applications," *J. Vac. Sci. Technol. A, Vac. Surf Films*, vol. 14, no. 3, pp. 913–918, May 1996.

[31] ——, "Optical bandgap of the ternary semiconductor SiGeC," *J. Appl. Phys.*, vol. 70, no. 4, pp. 2470–2472, Aug. 1991.

[32] R. A. Soref, Z. Atzman, F. Shaapur, M. Robinson, and R. Westhoff, "Infrared waveguiding in SiGeC upon silicon," *Opt. Lett.*, vol. 21, no. 5, p. 345, Mar. 1996.

[33] F. Y. Huang and K. L. Wang, "Normal-incidence epitaxial SiGeC photodetector near 1.3 μm wavelength grown on Si substrate," *Appl. Phys. Lett.*, vol. 69, no. 16, pp. 2330–2332, Oct. 1996.

[34] F. Y. Huang, K. Sakamoto, K. L. Wang, P. Trinh, and B. Jalali, "Epitaxial SiGeC waveguide photodetector grown on Si substrate with response in the 1.3–1.55-μm wavelength range," *IEEE Photon. Technol. Lett.*, vol. 9, no. 2, pp. 229–231, Feb. 1997.

[35] B. Li, S.-J. Chua, and E. A. Fitzgerald, "Theoretical analysis of $Si_{1-x-y}Ge_xC_y$ near-infrared photodetectors," *Opt. Eng.*, vol. 42, no. 7, p. 1993, 2003.

[36] J. W. Matthews and A. E. Blakeslee, "Defects in epitaxial multilayers, I: Misfit dislocations," *J. Cryst. Growth*, vol. 27, pp. 118–125, Dec. 1974.

[37] Z. Atzmon, A. E. Bair, E. J. Jaquez, J. W. Mayer, D. Chandrasekhar, D. J. Smith, R. L. Hervig, and M. Robinson, "Chemical vapor deposition of heteroepitaxial SiGeC films on Si substrates," *Appl. Phys. Lett.*, vol. 65, no. 20, pp. 2559–2561, Nov. 1994.

[38] M. Yang, C. Chang, and J. C. Sturm, "Band alignments and band gaps in SiGeC/Si structures," in *Silicon-Germanium-Carbon Alloys*, S. T. Pantellides and S. Zollner, Eds. New York: Taylor and Francis, 2002.

[39] L. Naval, B. Jalali, L. Gomelski, and J. M. Liu, "Optimization of SiGe/Si waveguide photodetectors operating at 1.3 μm," *J. Lightw. Technol.*, vol. 14, no. 4, pp. 787–797, May 1996.

[40] R. A. Soref and B. R. Bennett, "Electrooptical effects in silicon," *IEEE J. Quantum Electron.*, vol. QE-23, no. 1, pp. 123–129, Jan. 1987.

[41] R. Braunstein, A. Moore, and F. Herman, "Intrinsic optical absorption in germanium-silicon alloys," *Phys. Rev.*, vol. 109, no. 3, pp. 695–710, Feb. 1958.

[42] G. Cocorullo and I. Rendina, "Thermo-optical modulator at 1.5 μm in silicon etalon," *Electron. Lett.*, vol. 28, no. 1, pp. 83–85, Jan. 1992.

[43] M. J. Kerr and A. Cuevas, "General parameterization of Auger recombination in crystalline silicon," *J. Appl. Phys.*, vol. 91, no. 4, pp. 2473–2480, Feb. 2002.

[44] D. W. Winston, "Physical simulation of optoelectronic semiconductor devices," Ph.D. dissertation, Univ. Colorado, Boulder, CO, 1996.

[45] F. Schäffler, "Silicon-germanium ($Si_{1-x}Ge_x$)," in *Properties of Advanced Semiconductor Materials: GaN, AlN, InN, BN, SiC, SiGe*, M. E. Levinshtein, S. L. Rumyantsev, and M. S. Shur, Eds. New York: Wiley, 2001.

[46] M. M. Rieger and P. Vogl, "Electronic-band parameters in strained $Si_{1-x}Ge_x$ alloys on $Si_{1-y}Ge_y$ substrates," *Phys. Rev. B, Condens. Matter*, vol. 48, no. 19, p. 47, 1993.

[47] C. Y. Lin and C. W. Liu, "Hole effective masses in relaxed $Si_{1-x}C_x$ and $Si_{1-y}Ge_y$ alloys," *Appl. Phys. Lett.*, vol. 70, no. 11, pp. 1441–1443, 1997.

Martin F. Schubert (S'03) was born in Stuttgart, Germany, in 1982. He received the B.S. and M.Eng. degrees in electrical engineering, both from Cornell University, Ithaca, NY, in 2004 and 2005, respectively. He is currently working toward the Ph.D. degree in electrical engineering at Rensselaer Polytechnic Institute, Troy, NY.

His current research focuses on semiconductor optoelectronics.

Farhan Rana (M'99) was born in Karachi, Pakistan, in 1971. He received the B.S., M.S., and Ph.D. degrees from Massachusetts Institute of Technology, Cambridge, all in electrical engineering.

He worked on a variety of different topics related to semiconductor optoelectronics, quantum optics, and mesoscopic physics during his Ph.D. research. Before starting his doctoral studies, he worked with IBM's T.J. Watson Research Center, Yorktown Heights, NY, on silicon nanocrystal and quantum dot memory devices. After finishing his doctoral work in 2002, he joined the faculty of Electrical and Computer Engineering, Cornell University, Ithaca, NY. His current research focuses on semiconductor optoelectronics and quantum optics.

Dr. Rana received the U.S. National Science Foundation Faculty CAREER Award in 2004.